Neural-network-identification-based adaptive control of wing rock motions

C.-F. Hsu, C.-M. Lin and T.-Y. Chen

Abstract: The proposed control system comprises a computation controller and a tracking controller. The computation controller containing a recurrent neural network identifier is the principal controller, and the tracking controller is designed to achieve L_2 tracking performance with a desired attenuation level. To investigate the effectiveness of the proposed control system the design methodology is used to control a wing rock motion, manifested by a limit-cycle oscillation predominantly for an aircraft operating at subsonic speeds and high angles of attack. Simulation results demonstrate that the proposed control system can achieve favourable tracking performance for the wing rock motion.

1 Introduction

Neural-network-based control techniques have represented an alternative design direction for control problems [1–8]. The key element is the approximation theory, where the parameterised neural network identifier can approximate the unknown plant dynamic model after learning [1]. Based on this property the neural-network-based controllers have been developed to compensate for the effects of nonlinearities and system uncertainties, so that the stability, convergence and robustness of the control system can be improved. The basic issues of neural network control are to provide online learning algorithms that do not require preliminary offline tuning. Some of these online learning algorithms are based on the gradient descent method, and some are based on the Lyapunov stability theorem.

However, most of the neural networks are feedforward neural networks (FNNs); they belong to static mapping networks. Without the aid of tapped delays the FNNs are unable to represent a dynamic mapping. Although several approaches have used the FNNs with tapped delays to deal with dynamic systems these FNNs require a large number of neurons to represent dynamic responses [1]. On the other hand, the recurrent neural network (RNN) has capabilities superior to FNN, such as its dynamic response and its information storing ability [9]. Since the RNN has an internal feedback loop, it captures the dynamic response of a system with feedback through delays. Thus RNN is a dynamic mapping network. Several approaches have demonstrated that RNN is superior to FNN for system identification and control [9–12].

High-performance aircraft often require operating at subsonic speeds and high angles of attack. They may become unstable or enter into a self-induced limit cycle oscillation, mainly rolling motion known as wing rock motion [13]. The aerodynamic rolling moment is a complex nonlinear function. This wing rock motion is a concern because it may have adverse effects on maneuverability, tracking accuracy, and operational safety. Such oscillations lead to a significant loss in lift and can cause a serious safety problem during maneuvres such as landing or takeoff. The control of wing rock motion is significant importance. However, the underlying mechanism of the wing rock motion is still not very clear because with modern combat aircraft it is difficult to isolate the various flow phenomena.

Recently, several theoretical and experimental studies have been performed to understand the dynamics of the wing rock motion and to predict the amplitude and frequency of limit cycle oscillation [14–16]. A series of papers have considered the control of the wing rock motion based on output feedback linearisation theory and adaptive control technique [17–20]. In the feedback linearisation design approaches the feedback control gain should be preselected by trial and error to achieve the desired performance; however, this trial procedure is time-consuming and the system model is required [19, 20]. In the adaptive techniques, the knowledge of the structure of the aerodynamic functions is required; however, the structure is difficult to obtain [17, 18].

This paper develops a neural-network-identification-based adaptive control (NNIAC) system to achieve L_2 tracking performance for the wing rock motion. Since RNN captures the dynamic response, it is used to identify the unknown system dynamic function. All the weights of the RNN are tuned based on the Lyapunov function to achieve favourable identification performance. And, by the L_2 control design technique, the effects of the approximation error on the tracking performance can be attenuated to arbitrary specified level. The proposed NNIAC design method is applied for a wing rock motion control. Simulation results demonstrate that the developed NNIAC system can achieve favourable tracking performance without knowledge of the system dynamic function.

2 Problem statement of wing rock motion

The delta wing of an aircraft is represented schematically in Fig. 1. This delta wing has one degree of freedom, and the dynamical system includes the wing (a flat uniform plate)

IEE Proceedings online no. 20050904

doi: 10.1049/ip-cta:20050904

Paper first received 7th October 2002 and in revised form 20th May 2004

C.-F. Hsu is with the Department of Electrical and Control Engineering, National Chiao-Tung University, Hsinchu 300, Taiwan, Republic of China

C.-M. Lin and T.-Y. Chen are with the Department of Electrical Engineering, Yuan-Ze University, Chung-Li, Tao-Yuan 320, Taiwan, Republic of China

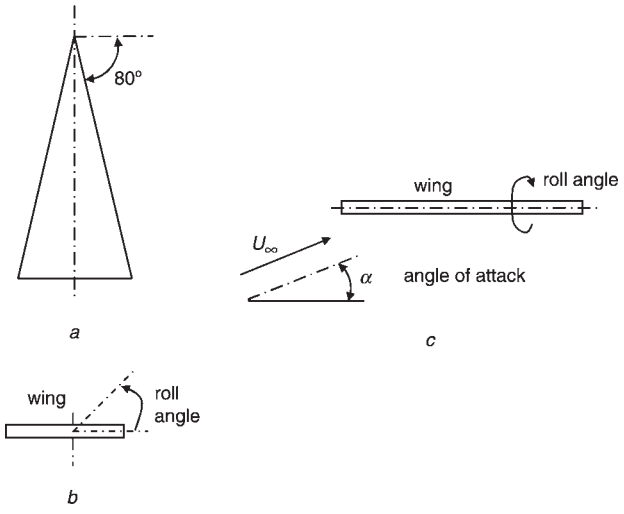

Fig. 1 *Scheme of delta wing*
a Plan view
b End view
c Side view

and the parts of the string that rotate with it. The aerodynamic rolling moment is a complex nonlinear function of the rolling angle, roll rate, angle of attack and sideslip angle. The nonlinear motion equation for an 80° slender delta wing has been developed by Elzebda *et al.* [13] as

$$\ddot{\phi} = \left(pU_\infty^2 Sb/2I_{xx}\right)C_l + u \tag{1}$$

where ϕ is the roll angle, an over-dot denotes a derivative with respect to time, u is the control effort which represents the aileron deflection, p is the density of air, U_∞ is the freestream velocity, S is the wing reference area, b is the chord, I_{xx} is the mass moment of inertia, and C_l is the roll moment coefficient. The roll-moment coefficient is written as [13]

$$C_l = c_0 + c_1\phi + c_2\dot{\phi} + c_3|\phi|\dot{\phi} + c_4|\dot{\phi}|\dot{\phi} + c_5\phi^3 \tag{2}$$

The aerodynamic parameters c_i, $i = 0, 1, \ldots, 5$ are nonlinear functions for different angles of attack [13, 14]. Substituting (2) into (1) yields

$$\ddot{\phi} = f(\phi, \dot{\phi}) + u \tag{3}$$

where

$$f(\phi, \dot{\phi}) = b_0 + b_1\phi + b_2\dot{\phi} + b_3|\phi|\dot{\phi} + b_4|\dot{\phi}|\dot{\phi} + b_5\phi^3 \tag{4}$$

and the parameters b_i, $i = 0, 1, \ldots, 5$ are given by

$$b_i = \left(pU_\infty^2 Sb/2I_{xx}\right)c_i \tag{5}$$

To observe the dynamic behaviour, the open-loop system time response with $u = 0$ was simulated for two initial conditions: a small initial condition $(\phi(0) = 6°, \dot{\phi}(0) = 3°/\text{s})$ and a large initial condition $(\phi(0) = 30°, \dot{\phi}(0) = 10°/\text{s})$. The phase-plane plots of these simulations are shown in Fig. 2. For the small initial condition a limit cycle oscillation is obtained, and for the large initial condition the roll angle is divergent. Thus, it is shown that the uncontrolled wing rock motion will be unstable for some initial conditions.

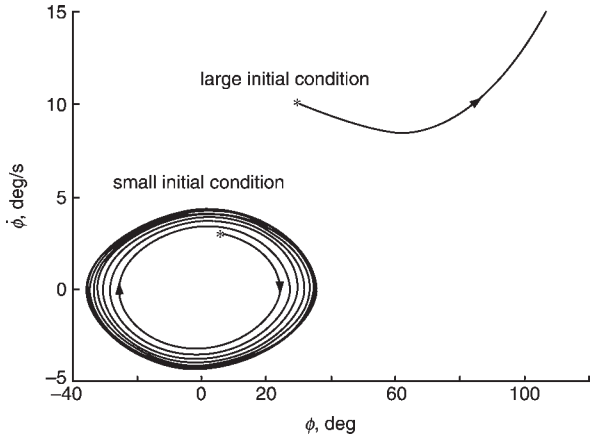

Fig. 2 *Phase-plane portraits of uncontrolled wing rock*

3 Neural-network-identification-based adaptive control

The control problem is to design a control system so that the output ϕ can track the command trajectory ϕ_m, where the tracking error vector is defined as

$$\boldsymbol{E} = [e \quad \dot{e}]^T = \left[\phi_m - \phi \quad \dot{\phi}_m - \dot{\phi}\right]^T \tag{6}$$

Assuming that the parameters of the wing rock motion system in (3) are well known, there exists an ideal controller as [21]

$$u_{id} = -f(\phi, \dot{\phi}) + \ddot{\phi}_m + k_2\dot{e} + k_1 e \tag{7}$$

Substituting (7) into (3) gives the following equation:

$$\ddot{e} + k_2\dot{e} + k_1 e = 0 \tag{8}$$

If k_1 and k_2 are chosen to correspond to the coefficients of a Hurwitz polynomial, it implies $\lim_{t\to\infty} e = 0$. However, the system dynamic function $f(\phi, \dot{\phi})$ in (7) is a nonlinear time-varying function and it cannot be obtained exactly, so the ideal controller u_{id} cannot be implemented.

3.1 Description of recurrent neural network identifier

To obtain the ideal controller an RNN identifier as shown in Fig. 3 is used to identify the unknown system dynamic function $f(\phi, \dot{\phi})$. The RNN maps according to

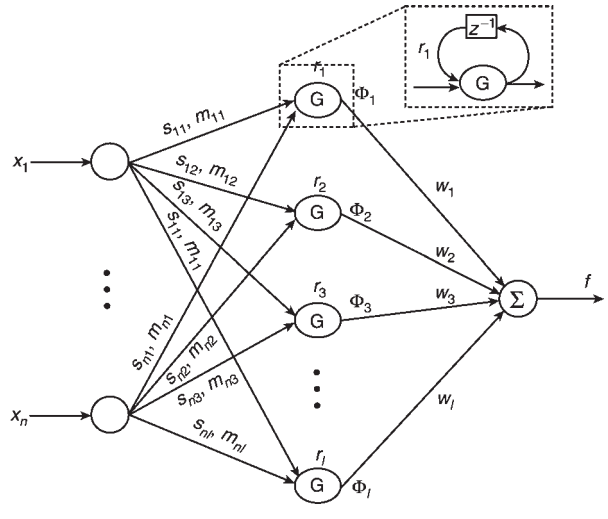

Fig. 3 *Network structure of recurrent neural network*

$$f(N) = \sum_{k=1}^{l} w_k \Phi_k(|x_i(N) - m_{ik}|, \delta_{ik}, r_k, \Phi_k(N-1)) \quad (9)$$

where x_i, $i = 1, 2, \ldots, n$ contain the input variables, N is the number of iterations, w_k represents the connective weights between the hidden layer and the output layer, Φ_k represents the firing weight of the kth neuron in the hidden layer, m_{ik} and δ_{ik} are the centre and width of the activation function, respectively, and r_k is the internal feedback gain. The firing weight can be represented as

$$\Phi_k(N) = e^{-net_k(N)} \quad (10)$$

where

$$net_k(N) = \sum_{i=1}^{n} \frac{[x_i(N) + \Phi_k(N-1)r_k - m_{ik}]^2}{\delta_{ik}^2} \quad (11)$$

or

$$net_k(N) = \sum_{i=1}^{n} s_{ik}^2 [x_i(N) + \Phi_k(N-1)r_k - m_{ik}]^2 \quad (12)$$

with $s_{ik} = 1/\delta_{ik}$ is the inverse radius of the radial basis function. For simplicity of discussion, define the vectors $\boldsymbol{m}$, $\boldsymbol{s}$ and $\boldsymbol{r}$ collecting all parameters of the hidden layer as

$$\boldsymbol{m} = [m_{11} \cdots m_{n1} \quad m_{12} \cdots m_{n2} \quad \cdots\cdots \quad m_{1l} \cdots m_{nl}]^T \quad (13)$$

$$\boldsymbol{s} = [s_{11} \cdots s_{n1} \quad s_{12} \cdots s_{n2} \quad \cdots\cdots \quad s_{1l} \cdots s_{nl}]^T \quad (14)$$

$$\boldsymbol{r} = [r_1 \cdots r_l]^T \quad (15)$$

Then the output of the RNN identifier can be represented in a vector form as [22]

$$\boldsymbol{f}(\boldsymbol{x}, \boldsymbol{m}, \boldsymbol{s}, \boldsymbol{r}, \boldsymbol{w}) = \boldsymbol{w}^T \boldsymbol{\Phi}(\boldsymbol{x}, \boldsymbol{m}, \boldsymbol{s}, \boldsymbol{r}) \quad (16)$$

where $\boldsymbol{x} = [x_1 \ x_2 \ \ldots \ x_n]^T$, $\boldsymbol{w} = [w_1 \ w_2 \ \ldots \ w_l]^T$ and $\boldsymbol{\Phi} = [\Phi_1 \ \Phi_2 \ \ldots \ \Phi_l]^T$. From the universal approximation theorem it has been proven that there exists an optimal RNN identifier such that it can uniformly approximate the unknown system dynamic function [22]. Thus,

$$\boldsymbol{f}(\phi, \dot{\phi}) = \boldsymbol{f}^*(\boldsymbol{x}, \boldsymbol{m}^*, \boldsymbol{s}^*, \boldsymbol{r}^*, \boldsymbol{w}^*) + \boldsymbol{\Delta} = \boldsymbol{w}^{*T} \boldsymbol{\Phi}^*(\boldsymbol{x}, \boldsymbol{m}^*, \boldsymbol{s}^*, \boldsymbol{r}^*) + \boldsymbol{\Delta} \quad (17)$$

where $\boldsymbol{\Delta}$ denotes a matching error, $\boldsymbol{w}^*$ and $\boldsymbol{\Phi}^*$ are the optimal parameter vectors of $\boldsymbol{w}$ and $\boldsymbol{\Phi}$, respectively, and $\boldsymbol{m}^*$, $\boldsymbol{s}^*$ and $\boldsymbol{r}^*$ are the optimal parameter vectors of $\boldsymbol{m}$, $\boldsymbol{s}$ and $\boldsymbol{r}$, respectively. The optimal weighting vectors $\boldsymbol{w}^*$, $\boldsymbol{m}^*$, $\boldsymbol{s}^*$ and $\boldsymbol{r}^*$ that are needed to best approximate the system dynamic function are difficult to determine. Thus an RNN identifier is defined as

$$\hat{\boldsymbol{f}} = \hat{\boldsymbol{w}}^T \hat{\boldsymbol{\Phi}}(\boldsymbol{x}, \hat{\boldsymbol{m}}, \hat{\boldsymbol{s}}, \hat{\boldsymbol{r}}) \quad (18)$$

where $\hat{\boldsymbol{w}}$ and $\hat{\boldsymbol{\Phi}}$ are the estimated vectors of $\boldsymbol{w}^*$ and $\boldsymbol{\Phi}^*$, respectively, and $\hat{\boldsymbol{m}}$, $\hat{\boldsymbol{s}}$ and $\hat{\boldsymbol{r}}$ are the estimated vectors of $\boldsymbol{m}^*$, $\boldsymbol{s}^*$ and $\boldsymbol{r}^*$, respectively. Define the estimated error $\tilde{\boldsymbol{f}}$ as

$$\tilde{\boldsymbol{f}} = \boldsymbol{f} - \hat{\boldsymbol{f}} = \tilde{\boldsymbol{w}}^T \hat{\boldsymbol{\Phi}} + \hat{\boldsymbol{w}}^T \tilde{\boldsymbol{\Phi}} + \tilde{\boldsymbol{w}}^T \tilde{\boldsymbol{\Phi}} + \boldsymbol{\Delta} \quad (19)$$

where $\tilde{\boldsymbol{w}} = \boldsymbol{w}^* - \hat{\boldsymbol{w}}$ and $\tilde{\boldsymbol{\Phi}} = \boldsymbol{\Phi}^* - \hat{\boldsymbol{\Phi}}$. In the following, some tuning laws are developed to tune online the weights of the RNN to achieve favourable identification of the system dynamic function. To achieve this goal the Taylor expansion linearisation technique is employed to transform the nonlinear activation function into a partially linear form, i.e. [23]

$$\tilde{\boldsymbol{\Phi}} = \begin{bmatrix} \tilde{\Phi}_1 \\ \tilde{\Phi}_2 \\ \vdots \\ \tilde{\Phi}_l \end{bmatrix} = \begin{bmatrix} \frac{\partial \Phi_1}{\partial m} \\ \frac{\partial \Phi_2}{\partial m} \\ \vdots \\ \frac{\partial \Phi_l}{\partial m} \end{bmatrix} |_{m=\hat{m}} \tilde{\boldsymbol{m}} + \begin{bmatrix} \frac{\partial \Phi_1}{\partial s} \\ \frac{\partial \Phi_2}{\partial s} \\ \vdots \\ \frac{\partial \Phi_l}{\partial s} \end{bmatrix} |_{s=\hat{s}} \tilde{\boldsymbol{s}} + \begin{bmatrix} \frac{\partial \Phi_1}{\partial r} \\ \frac{\partial \Phi_2}{\partial r} \\ \vdots \\ \frac{\partial \Phi_l}{\partial r} \end{bmatrix} |_{r=\hat{r}} \tilde{\boldsymbol{r}} + \boldsymbol{h} \quad (20)$$

or

$$\tilde{\boldsymbol{\Phi}} = \boldsymbol{A}^T \tilde{\boldsymbol{m}} + \boldsymbol{B}^T \tilde{\boldsymbol{s}} + \boldsymbol{C}^T \tilde{\boldsymbol{r}} + \boldsymbol{h} \quad (21)$$

where $\tilde{\boldsymbol{m}} = \boldsymbol{m}^* - \hat{\boldsymbol{m}}$, $\tilde{\boldsymbol{s}} = \boldsymbol{s}^* - \hat{\boldsymbol{s}}$, $\tilde{\boldsymbol{r}} = \boldsymbol{r}^* - \hat{\boldsymbol{r}}$, $\boldsymbol{h}$ is a vector of higher-order terms,

$$\boldsymbol{A} = \left[\frac{\partial \Phi_1}{\partial m} \ \frac{\partial \Phi_2}{\partial m} \ \cdots \ \frac{\partial \Phi_l}{\partial m} \right] |_{m=\hat{m}},$$

$$\boldsymbol{B} = \left[\frac{\partial \Phi_1}{\partial s} \ \frac{\partial \Phi_2}{\partial s} \ \cdots \ \frac{\partial \Phi_l}{\partial s} \right] |_{s=\hat{s}}, \ \boldsymbol{C} = \left[\frac{\partial \Phi_1}{\partial r} \ \frac{\partial \Phi_2}{\partial r} \ \cdots \ \frac{\partial \Phi_l}{\partial r} \right] |_{r=\hat{r}}$$

and $\partial \Phi_k / \partial m$, $\partial \Phi_k / \partial s$ and $\partial \Phi_k / \partial r$ are defined as

$$\left[\frac{\partial \Phi_k}{\partial m} \right]^T = \left[\underbrace{0 \cdots 0}_{(k-1)\times l} \ \frac{\partial \Phi_k}{\partial m_{1k}} \ \cdots \ \frac{\partial \Phi_k}{\partial m_{nk}} \ \underbrace{0 \cdots 0}_{(l-k)\times l} \right] \quad (22)$$

$$\left[\frac{\partial \Phi_k}{\partial s} \right]^T = \left[\underbrace{0 \cdots 0}_{(k-1)\times l} \ \frac{\partial \Phi_k}{\partial s_{1k}} \ \cdots \ \frac{\partial \Phi_k}{\partial s_{nk}} \ \underbrace{0 \cdots 0}_{(l-k)\times l} \right] \quad (23)$$

$$\left[\frac{\partial \Phi_k}{\partial \boldsymbol{r}} \right]^T = \left[\underbrace{0 \cdots 0}_{(k-1)} \ \frac{\partial \Phi_k}{\partial r_k} \ \underbrace{0 \cdots 0}_{(l-k)} \right] \quad (24)$$

Substituting (21) into (19) gives

$$\begin{aligned} \tilde{\boldsymbol{f}} &= \tilde{\boldsymbol{w}}^T \hat{\boldsymbol{\Phi}} + \hat{\boldsymbol{w}}^T (\boldsymbol{A}^T \tilde{\boldsymbol{m}} + \boldsymbol{B}^T \tilde{\boldsymbol{s}} + \boldsymbol{C}^T \tilde{\boldsymbol{r}} + \boldsymbol{h}) + \tilde{\boldsymbol{w}}^T \tilde{\boldsymbol{\Phi}} + \boldsymbol{\Delta} \\ &= \tilde{\boldsymbol{w}}^T \hat{\boldsymbol{\Phi}} + \tilde{\boldsymbol{m}}^T \boldsymbol{A} \hat{\boldsymbol{w}} + \tilde{\boldsymbol{s}}^T \boldsymbol{B} \hat{\boldsymbol{w}} + \tilde{\boldsymbol{r}}^T \boldsymbol{C} \hat{\boldsymbol{w}} + \varepsilon \end{aligned} \quad (25)$$

where $\hat{\boldsymbol{w}}^T \boldsymbol{A}^T \tilde{\boldsymbol{m}} = \tilde{\boldsymbol{m}}^T \boldsymbol{A} \hat{\boldsymbol{w}}$, $\hat{\boldsymbol{w}}^T \boldsymbol{B}^T \tilde{\boldsymbol{s}} = \tilde{\boldsymbol{s}}^T \boldsymbol{B} \hat{\boldsymbol{w}}$ and $\hat{\boldsymbol{w}}^T \boldsymbol{C}^T \tilde{\boldsymbol{r}} = \tilde{\boldsymbol{r}}^T \boldsymbol{C} \hat{\boldsymbol{w}}$ are used since they are scales, and the approximation error $\boldsymbol{\varepsilon} = \hat{\boldsymbol{w}}^T \boldsymbol{h} + \tilde{\boldsymbol{w}}^T \tilde{\boldsymbol{\Phi}} + \boldsymbol{\Delta}$.

3.2 Adaptive controller design

The NNIAC wing rock motion control system is shown in Fig. 4, where the adaptive controller comprises a computation controller and a tracking controller as

$$u_{ac} = u_{cp} + u_{tr} \quad (26)$$

where the computation controller is chosen as

$$u_{cp} = -\hat{f} + \ddot{\phi}_m + k_2 \dot{e} + k_1 e \quad (27)$$

By substituting (26) into (3) and using (25), the tracking error dynamic equation can be obtained as follows:

$$\begin{aligned} \dot{\boldsymbol{E}} &= \boldsymbol{A}_m \boldsymbol{E} - \boldsymbol{d}_m (f - \hat{f} + u_{tr}) \\ &= \boldsymbol{A}_m \boldsymbol{E} - \boldsymbol{d}_m (\tilde{\boldsymbol{w}}^T \hat{\boldsymbol{\Phi}} + \tilde{\boldsymbol{m}}^T \boldsymbol{A} \hat{\boldsymbol{w}} + \tilde{\boldsymbol{s}}^T \boldsymbol{B} \hat{\boldsymbol{w}} + \tilde{\boldsymbol{r}}^T \boldsymbol{C} \hat{\boldsymbol{w}} + \varepsilon + u_{tr}) \end{aligned} \quad (28)$$

where

$$\boldsymbol{A}_m = \begin{bmatrix} 0 & 1 \\ -k_1 & -k_2 \end{bmatrix}$$

and $\boldsymbol{d}_m = [0 \quad 1]^T$. The following theorem shows the properties of this adaptive control system.

Theorem 1: Consider a wing rock motion system (3) with the control (26). In the computation controller (27), the

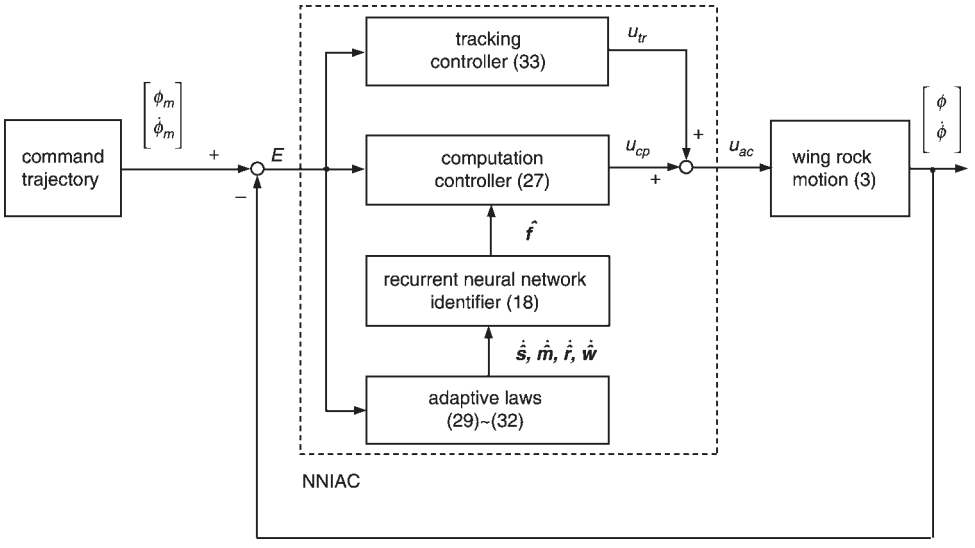

Fig. 4 *Neural-network-identification-based adaptive control wing rock motion system*

adaptation laws of the recurrent neural network identifier are designed as

$$\dot{\hat{\boldsymbol{w}}} = -\dot{\tilde{\boldsymbol{w}}} = -\eta_1 \boldsymbol{E}^T \boldsymbol{P} \boldsymbol{d}_m \hat{\boldsymbol{\Phi}} \tag{29}$$

$$\dot{\hat{\boldsymbol{m}}} = -\dot{\tilde{\boldsymbol{m}}} = -\eta_2 \boldsymbol{E}^T \boldsymbol{P} \boldsymbol{d}_m \boldsymbol{A} \hat{\boldsymbol{w}} \tag{30}$$

$$\dot{\hat{\boldsymbol{s}}} = -\dot{\tilde{\boldsymbol{s}}} = -\eta_3 \boldsymbol{E}^T \boldsymbol{P} \boldsymbol{d}_m \boldsymbol{B} \hat{\boldsymbol{w}} \tag{31}$$

$$\dot{\hat{\boldsymbol{r}}} = -\dot{\tilde{\boldsymbol{r}}} = -\eta_4 \boldsymbol{E}^T \boldsymbol{P} \boldsymbol{d}_m \boldsymbol{C} \hat{\boldsymbol{w}} \tag{32}$$

and the tracking controller is designed as

$$u_{tr} = \frac{1}{\kappa} \boldsymbol{d}_m^T \boldsymbol{P} \boldsymbol{E} \tag{33}$$

where η_1, η_2, η_3 and η_4 are the learning rates with positive constants and the symmetry positive definite matrix $\boldsymbol{P}$ and the positive definite matrix $\boldsymbol{Q}$ satisfy the following Riccati-like equation

$$\boldsymbol{P}\boldsymbol{A}_m + \boldsymbol{A}_m^T \boldsymbol{P} + \boldsymbol{Q} - \frac{2}{\kappa} \boldsymbol{P} \boldsymbol{d}_m \boldsymbol{d}_m^T \boldsymbol{P} + \frac{1}{\rho^2} \boldsymbol{P} \boldsymbol{d}_m \boldsymbol{d}_m^T \boldsymbol{P} = 0 \tag{34}$$

where $2\rho^2 \geq \kappa$. Then the overall control system shown in Fig. 4 gurantees the following property:

$$\int_0^t \boldsymbol{E}^T \boldsymbol{Q} \boldsymbol{E} d\tau \leq \boldsymbol{E}^T(0) \boldsymbol{P} \boldsymbol{E}(0) + \frac{\tilde{\boldsymbol{w}}^T(0)\tilde{\boldsymbol{w}}(0)}{\eta_1} + \frac{\tilde{\boldsymbol{m}}^T(0)\tilde{\boldsymbol{m}}(0)}{\eta_2} + \frac{\tilde{\boldsymbol{s}}^T(0)\tilde{\boldsymbol{s}}(0)}{\eta_3} + \frac{\tilde{\boldsymbol{r}}^T(0)\tilde{\boldsymbol{r}}(0)}{\eta_4} + \rho^2 \int_0^t \varepsilon^2 d\tau \tag{35}$$

for all $t \geq 0$, where κ is a design gain and ρ is an attenuation level.

Proof: Consider a Lyapunov function in the form

$$V(\boldsymbol{E},\ \tilde{\boldsymbol{w}},\ \tilde{\boldsymbol{m}},\ \tilde{\boldsymbol{s}},\ \tilde{\boldsymbol{r}}) = \frac{1}{2} \boldsymbol{E}^T \boldsymbol{P} \boldsymbol{E} + \frac{\tilde{\boldsymbol{w}}^T \tilde{\boldsymbol{w}}}{2\eta_1} + \frac{\tilde{\boldsymbol{m}}^T \tilde{\boldsymbol{m}}}{2\eta_2} + \frac{\tilde{\boldsymbol{s}}^T \tilde{\boldsymbol{s}}}{2\eta_3} + \frac{\tilde{\boldsymbol{r}}^T \tilde{\boldsymbol{r}}}{2\eta_4} \tag{36}$$

Differentiating (36) with respect to time and using (29)–(32) obtains

$$\begin{aligned}
\dot{\boldsymbol{V}}(\boldsymbol{E},\ \tilde{\boldsymbol{w}},\ \tilde{\boldsymbol{m}},\ \tilde{\boldsymbol{s}},\ \tilde{\boldsymbol{r}}) &= \frac{1}{2}\dot{\boldsymbol{E}}^T \boldsymbol{P} \boldsymbol{E} + \frac{1}{2}\boldsymbol{E}^T \boldsymbol{P} \dot{\boldsymbol{E}} + \frac{\tilde{\boldsymbol{w}}^T \dot{\tilde{\boldsymbol{w}}}}{\eta_1} + \frac{\tilde{\boldsymbol{m}}^T \dot{\tilde{\boldsymbol{m}}}}{\eta_2} + \frac{\tilde{\boldsymbol{s}}^T \dot{\tilde{\boldsymbol{s}}}}{\eta_3} + \frac{\tilde{\boldsymbol{r}}^T \dot{\tilde{\boldsymbol{r}}}}{\eta_4} \\
&= \frac{1}{2}\boldsymbol{E}^T (\boldsymbol{A}_m^T \boldsymbol{P} + \boldsymbol{P}\boldsymbol{A}_m)\boldsymbol{E} + \frac{\tilde{\boldsymbol{w}}^T \dot{\tilde{\boldsymbol{w}}}}{\eta_1} + \frac{\tilde{\boldsymbol{m}}^T \dot{\tilde{\boldsymbol{m}}}}{\eta_2} + \frac{\tilde{\boldsymbol{s}}^T \dot{\tilde{\boldsymbol{s}}}}{\eta_3} + \frac{\tilde{\boldsymbol{r}}^T \dot{\tilde{\boldsymbol{r}}}}{\eta_4} \\
&\quad - \boldsymbol{E}^T \boldsymbol{P} \boldsymbol{d}_m (\tilde{\boldsymbol{w}}^T \hat{\boldsymbol{\Phi}} + \tilde{\boldsymbol{m}}^T \boldsymbol{A} \hat{\boldsymbol{w}} + \tilde{\boldsymbol{s}}^T \boldsymbol{B} \hat{\boldsymbol{w}} + \tilde{\boldsymbol{r}}^T \boldsymbol{C} \hat{\boldsymbol{w}} + \varepsilon + u_{tr}) \\
&= \frac{1}{2}\boldsymbol{E}^T (\boldsymbol{A}_m^T \boldsymbol{P} + \boldsymbol{P}\boldsymbol{A}_m)\boldsymbol{E} - \tilde{\boldsymbol{w}}^T \left(\boldsymbol{E}^T \boldsymbol{P} \boldsymbol{d}_m \hat{\boldsymbol{\Phi}} - \frac{\dot{\hat{\boldsymbol{w}}}}{\eta_1} \right) \\
&\quad - \tilde{\boldsymbol{m}}^T \left(\boldsymbol{E}^T \boldsymbol{P} \boldsymbol{d}_m \boldsymbol{A} \hat{\boldsymbol{w}} - \frac{\dot{\hat{\boldsymbol{m}}}}{\eta_2} \right) - \tilde{\boldsymbol{s}}^T \left(\boldsymbol{E}^T \boldsymbol{P} \boldsymbol{d}_m \boldsymbol{B} \hat{\boldsymbol{w}} - \frac{\dot{\hat{\boldsymbol{s}}}}{\eta_3} \right) \\
&\quad - \tilde{\boldsymbol{r}}^T \left(\boldsymbol{E}^T \boldsymbol{P} \boldsymbol{d}_m \boldsymbol{C} \hat{\boldsymbol{w}} - \frac{\dot{\hat{\boldsymbol{r}}}}{\eta_4} \right) - \boldsymbol{E}^T \boldsymbol{P} \boldsymbol{d}_m (\varepsilon + u_{tr}) \\
&= \frac{1}{2}\boldsymbol{E}^T (\boldsymbol{A}_m^T \boldsymbol{P} + \boldsymbol{P}\boldsymbol{A}_m)\boldsymbol{E} - \boldsymbol{E}^T \boldsymbol{P} \boldsymbol{d}_m (\varepsilon + u_{tr})
\end{aligned} \tag{37}$$

Using (33) and (34), (37) can be rewritten as

$$\begin{aligned}
\dot{\boldsymbol{V}}(\boldsymbol{E}, \tilde{\boldsymbol{w}}, \tilde{\boldsymbol{m}}, \tilde{\boldsymbol{s}}, \tilde{\boldsymbol{r}}) &= \frac{1}{2}\boldsymbol{E}^T \left(\boldsymbol{A}_m^T \boldsymbol{P} + \boldsymbol{P}\boldsymbol{A}_m - \frac{2}{\kappa} \boldsymbol{P} \boldsymbol{d}_m \boldsymbol{d}_m^T \boldsymbol{P} \right) \boldsymbol{E} \\
&\quad - \frac{1}{2}\varepsilon^T \boldsymbol{d}_m^T \boldsymbol{P} \boldsymbol{E} - \frac{1}{2}\boldsymbol{E}^T \boldsymbol{P} \boldsymbol{d}_m \varepsilon \\
&= \frac{1}{2}\boldsymbol{E}^T \left(-\boldsymbol{Q} - \frac{1}{\rho^2} \boldsymbol{P} \boldsymbol{d}_m \boldsymbol{d}_m^T \boldsymbol{P} \right) \boldsymbol{E} - \frac{1}{2}\varepsilon^T \boldsymbol{d}_m^T \boldsymbol{P} \boldsymbol{E} - \frac{1}{2}\boldsymbol{E}^T \boldsymbol{P} \boldsymbol{d}_m \varepsilon \\
&= -\frac{1}{2}\boldsymbol{E}^T \boldsymbol{Q} \boldsymbol{E} - \frac{1}{2}\left(\frac{1}{\rho} \boldsymbol{d}_m^T \boldsymbol{P} \boldsymbol{E} + \rho\varepsilon \right)^T \left(\frac{1}{\rho} \boldsymbol{d}_m^T \boldsymbol{P} \boldsymbol{E} + \rho\varepsilon \right) + \frac{1}{2}\rho^2 \varepsilon^2 \\
&\leq -\frac{1}{2}\boldsymbol{E}^T \boldsymbol{Q} \boldsymbol{E} + \frac{1}{2}\rho^2 \varepsilon^2
\end{aligned} \tag{38}$$

where $\left(\frac{1}{\rho} \boldsymbol{d}_m^T \boldsymbol{P} \boldsymbol{E} + \rho\varepsilon \right)^T \left(\frac{1}{\rho} \boldsymbol{d}_m^T \boldsymbol{P} \boldsymbol{E} + \rho\varepsilon \right) \geq 0$ and $\varepsilon^T \boldsymbol{d}_m^T \boldsymbol{P} \boldsymbol{E} = \boldsymbol{E}^T \boldsymbol{P} \boldsymbol{d}_m \varepsilon$ are used. Integrating both sides of (38) yields

$$V(t) - V(0) \leq -\frac{1}{2} \int_0^t \boldsymbol{E}^T \boldsymbol{Q} \boldsymbol{E} d\tau + \frac{1}{2}\rho^2 \int_0^t \varepsilon^2 d\tau \tag{39}$$

Since $V(t) \geq 0$, (39) implies the following inequality

$$\frac{1}{2}\int_0^t \boldsymbol{E}^T\boldsymbol{Q}\boldsymbol{E}\,d\tau \le V(0)+\frac{1}{2}\rho^2\int_0^t \varepsilon^2 d\tau$$
$$=\frac{1}{2}\boldsymbol{E}^T(0)\boldsymbol{P}\boldsymbol{E}(0)+\frac{\tilde{\boldsymbol{w}}^T(0)\tilde{\boldsymbol{w}}(0)}{2\eta_1}$$
$$+\frac{\tilde{\boldsymbol{m}}^T(0)\tilde{\boldsymbol{m}}(0)}{2\eta_2}+\frac{\tilde{\boldsymbol{s}}^T(0)\tilde{\boldsymbol{s}}(0)}{2\eta_3}$$
$$+\frac{\tilde{\boldsymbol{r}}^T(0)\tilde{\boldsymbol{r}}(0)}{2\eta_4}+\frac{1}{2}\rho^2\int_0^t \varepsilon^2 d\tau \qquad (40)$$

Thus the inequality (35) is proved.

4 Simulation results

The aerodynamic parameters of the delta wing for 25° angle of attack are used for simulations. It is assumed that $U_\infty = 15\,\text{m/s}$ and $b = 0.429\,\text{m}$. The parameter b_i for the aerodynamic coefficients in (3) are given by $b_0 = 0$, $b_1 = -0.01859521$, $b_2 = 0.015162375$, $b_3 = -0.06245153$, $b_4 = 0.00954708$ and $b_5 = 0.02145291$ [13, 17]. For a choice of $\boldsymbol{Q} = -\boldsymbol{I}$, solving the Riccati-like (34) with $2\rho^2 = \kappa$, we have

$$\boldsymbol{P} = \begin{bmatrix} 1.7625 & 0.7812 \\ 0.7812 & 0.8088 \end{bmatrix} \qquad (41)$$

The derivation of the NNIAC system does not need the use of aerodynamic parameters on the structure of the aerodynamic functions. The system parameters given are used only for simulations. To investigate the effectiveness of the developed control system, two initial conditions (small initial condition $\phi(0) = 6°$, $\dot{\phi}(0) = 3°/\text{s}$ and large initial condition $\phi(0) = 30°$, $\dot{\phi}(0) = 10°/\text{s}$) are simulated.

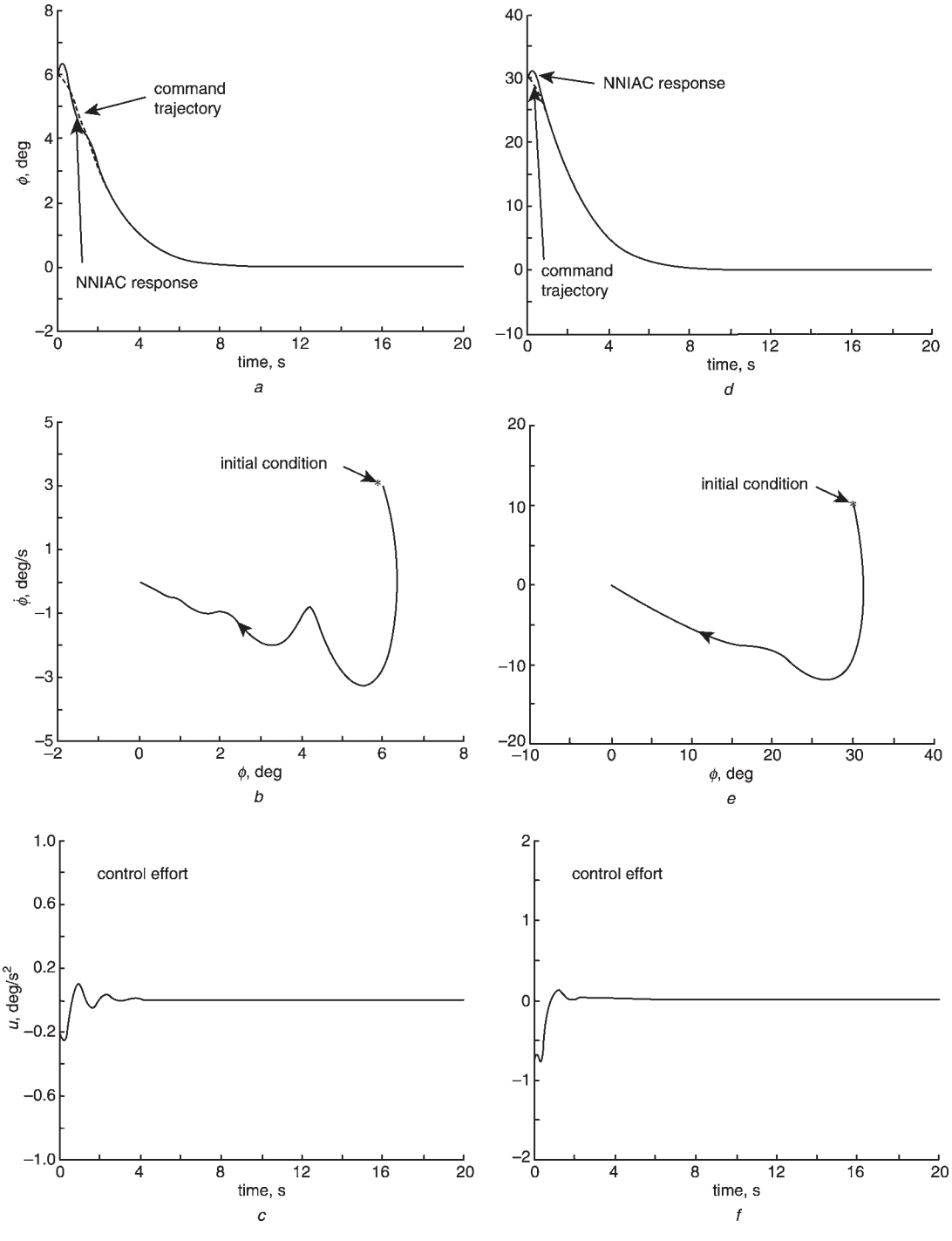

Fig. 5 *Time responses of NNIAC wing rock motion with $\kappa = 1$*

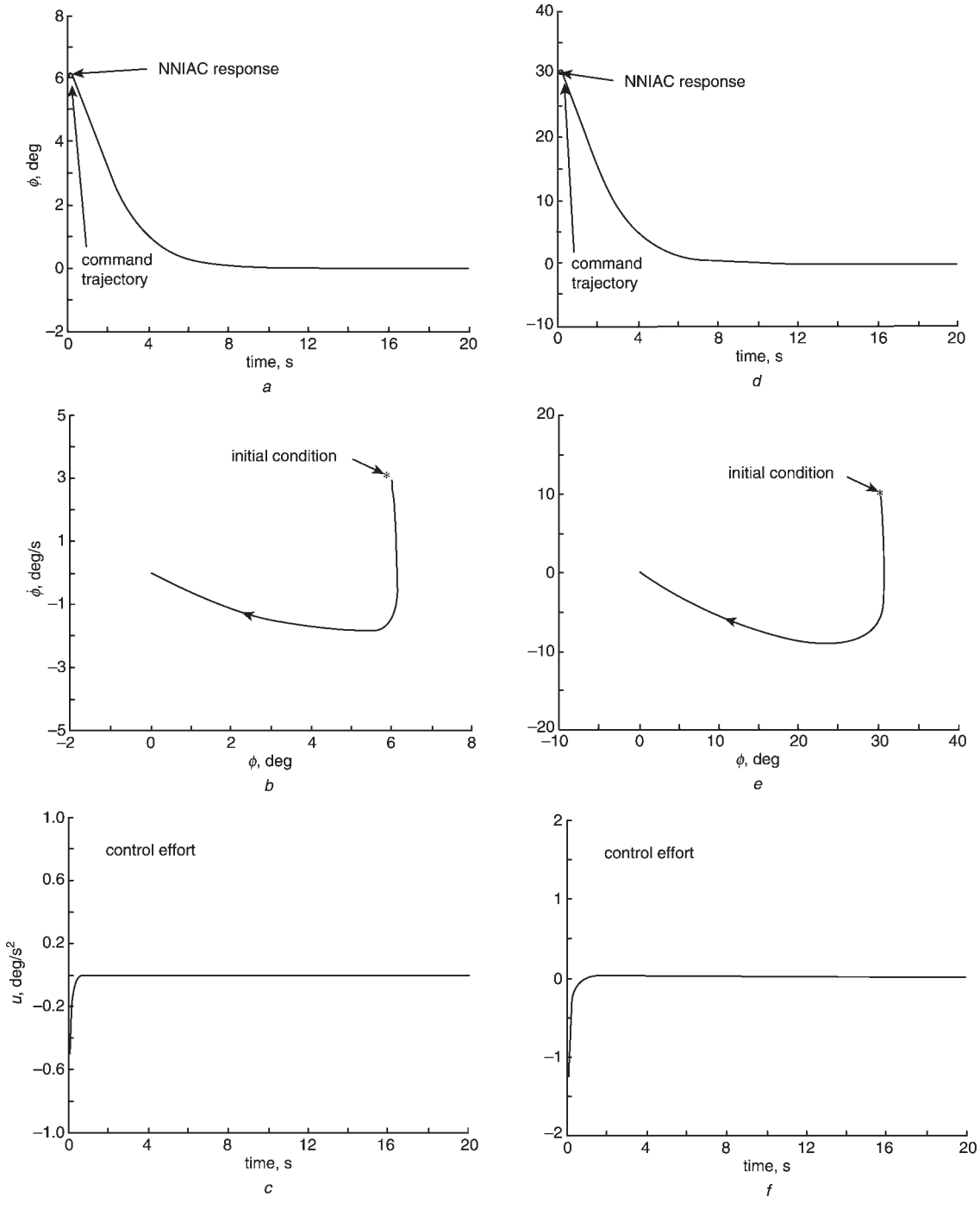

Fig. 6 *Time responses of NNIAC wing rock motion with $\kappa = 0.1$*

The control parameters and learning rates are selected as $k_1 = 0.64$, $k_2 = 1.6$, $\eta_1 = 20$, $\eta_2 = 20$, $\eta_3 = 20$ and $\eta_4 = 20$. All these parameters are chosen through trials to achieve favourable transient control performance and the requirement of stability.

The simulation results of the NNIAC system with $\kappa = 1$ for small and large initial conditions are shown in Fig. 5. The state responses are shown in Figs. 5*a* and 5*d*, the phase-plane portraits in Figs. 5*b* and 5*e*, and the associated control efforts in Figs. 5*c* and 5*f* for small and large initial conditions, respectively. Simulation results show that the satisfactory tracking performance of the NNIAC system has been achieved for the different initial conditions. To achieve a small attenuation level via the L_2 design technique, κ is reduced to 0.1.

The simulation results of the NNIAC system with $\kappa = 0.1$ for small and large initial conditions are shown in Fig. 6. The state responses are shown in Figs. 6*a* and 6*d*, the phase-plane portraits in Figs. 6*b* and 6*e*, and the associated control efforts in Figs. 6*c* and 6*f* for small and large initial conditions, respectively. From these simulation results it can be seen that favourable tracking performance can be achieved without any knowledge of system dynamic functions; moreover, it can achieve better performance of the system as the design gain κ is decreased.

5 Conclusions

This paper has developed a neural-network-identification-based adaptive control (NNIAC) system to attenuate the effects of the approximation error on the tracking performance using the L_2 tracking technique. The NNIAC system comprised a computation controller and a tracking controller. The computation controller including an RNN

identifier mimics the ideal controller and the tracking controller attenuats the effects of the approximation error. The NNIAC system developed is used to control a wing rock motion to demonstrate its effectiveness. Simulation results indicate that a small attenuation level can be achieved if the design gain κ is chosen to be small. However, this may lead to a large control signal. This situation is a trade-off between the amplitude of control signal and the performance of tracking error by choosing the design gain κ.

6 Acknowledgments

This work was partially supported by the National Science Council of the Republic of China under grant NSC 90-2213-E-155-016. The authors are grateful to the associate editor and to the reviewers for their valuable comments.

7 References

1 Narendra, K.S., and Parthasarathy, K.: 'Indentification and control of dynamical systems using networks', *IEEE Trans. Neural Netw.*, 1990, **1**, (1), pp. 4–27
2 Polycarpou, M.: 'Stable adaptive neural control scheme for nonlinear systems', *IEEE Trans. Autom. Control*, 1996, **41**, (3), pp. 447–451
3 Chak, C.K., Feng, G., and Ma, J.: 'An adaptive fuzzy neural network for MIMO system model approximation in high-dimensional space', *IEEE Trans. Syst. Man Cybern. B. Cybern.*, 1998, **28**, (3), pp. 436–446
4 Harris, C.J., Lee, T.H., and Ge, S.S.: 'Adaptive neural network control for robotic manipulators' (World Scientific, New Jersey, 1999)
5 Diao, Y., and Passino, K.M.: 'Stable fault-tolerant adaptive fuzzy/neural control for a turbine engine', *IEEE Trans. Control Syst. Technol.*, 2001, **9**, (3), pp. 494–509
6 Li, Y., Sundararajan, N., and Saratchandran, P.: 'Stable neuro-flight-controller using fully tuned radial basis function neural networks', *J. Guid. Control, Dyn.*, 2001, **24**, (4), pp. 665–674
7 Spooner, J.T., Maggiore, M., Ordonez, R., and Passino, K.M.: 'Stable adaptive control and estimation for nonlinear systems: neural and fuzzy approximation techniques' (Wiley, NY, 2002)
8 Lin, C.M., and Hsu, C.F.: 'Neural-network-based adaptive control for induction servomotor drive system', *IEEE Trans. Ind. Electron.*, 2002, **49**, (1), pp. 144–156
9 Ku, C.C., and Lee, K.Y.: 'Diagonal recurrent neural networks for dynamic systems control', *IEEE Trans. Neural Netw.*, 1995, **6**, (1), pp. 144–156
10 Lee, C.H., and Teng, C.C.: 'Indentification and control of dynamic systems using recurrent fuzzy neural networks', *IEEE Trans. Fuzzy Syst.*, 2000, **8**, (4), pp. 349–366
11 Chow, T.W.S., and Fang, Y.: 'A recurrent neural-network-based real-time learning control strategy applying to nonlinear systems with unknown dynamics', *IEEE Trans. Ind. Electron.*, 1998, **45**, (1), pp. 151–161
12 Lin, C.M., and Hsu, C.F.: 'Neural-network hybrid control for antilock braking systems', *IEEE Trans. Neural Netw.*, 2003, **14**, (2), pp. 351–359
13 Elzebda, J.M., Nayfeh, A.H., and Mook, D.T.: 'Development of an analytical model of wing rock for slender delta wings', *J. Aircraft*, 1989, **26**, (9), pp. 737–743
14 Nayfeh, A.H., Elzebda, J.M., and Mook, D.T.: 'Analytical study of the subsonic wing-rock phenomenon for slender delta wings', *J. Aircraft*, 1989, **26**, (9), pp. 805–809
15 Lan, C.E., Chen, Y., and Lin, K.J.: 'Experimental and analytical investigations of transonic limit-cycle oscillations of a flaperon', *J. Aircraft*, 1995, **32**, (5), pp. 905–910
16 Yang, G., Lu, X., and Zhuang, L.: 'Nonlinear analysis of dynamic stability and the prediction of wing rock', *J. Aircraft*, 2002, **39**, (1), pp. 84–90
17 Singh, S.N., Yim, W., and Wells, W.R.: 'Direct adaptive and neural control of wing-rock motion of slender delta wings', *J. Guid., Control Dyn.*, 1995, **18**, (1), pp. 25–30
18 Monahemi, M.M., and Krstic, M.: 'Control of wing rock motion using adaptive feedback linearization', *J. Guid., Control Dyn.*, 1996, **19**, (5), pp. 905–912
19 Shue, S.P., Sawan, M.E., and Rokhsaz, K.: 'Optimal feedback control of a nonlinear system: wing rock example', *J. Guid., Control Dyn.*, 1996, **19**, (1), pp. 166–171
20 Shue, S.P., and Agarwal, R.K.: 'Nonlinear H_∞ method for control of wing rock motions', *J. Guid. Control Dyn.*, 2000, **23**, (1), pp. 60–68
21 Slotine, J.E., and Li, W.: 'Applied nonlinear control' (Prentice-Hall, Englewood Cliffs, NJ, 1991)
22 Wang, L.X.: 'Adaptive fuzzy systems and control: design and stability analysis' (Prentice-Hall, Englewood Cliffs, NJ, 1994)
23 Wang, S.D., and Lin, C.K.: 'Adaptive tuning of fuzzy controller for robots', *Fuzzy Set Syst.*, 2002, **110**, (3), pp. 351–363